Development of β-TCP-Ti6Al4V structures: Driving cellular response by modulating physical and chemical properties

M.M. Costa[a,*], R. Lima[c,d], F. Melo-Fonseca[a,b], F. Bartolomeu[a], N. Alves[e], A. Miranda[c,d], M. Gasik[f], F.S. Silva[a], N.A. Silva[c,d], G. Miranda[a]

[a] Center for Micro-Electro Mechanical Systems (CMEMS-UMinho), University of Minho, Campus de Azurém, 4800-058 Guimarães, Portugal
[b] MIT Portugal Program, School of Engineering, University of Minho, Guimarães, Portugal
[c] Life and Health Sciences Research Institute (ICVS), School of Medicine, University of Minho, Campus de Gualtar, 4710-057 Braga, Portugal
[d] ICVS/3B's - PT Government Associate Laboratory, Braga/Guimarães, Portugal
[e] Center for Rapid and Sustainable Product Development (CDRSP), Polytechnic Institute of Leiria, Rua General Norton de Matos, Apartado 4133, 2411-901 Leiria, Portugal
[f] Department of Chemical and Metallurgical Engineering, School of Chemical Engineering, Aalto University Foundation, 00076 Aalto, Espoo, Finland

ARTICLE INFO

ABSTRACT

Load-bearing implants success is strongly dependent on several physical and chemical properties that are known to drive cellular response. In this work, multi-material β-TCP-Ti6Al4V cellular structures were designed to combine Ti6Al4V mechanical properties and β-Tricalcium Phosphate bioactivity, in order to promote bone ingrowth as the bioactive material is being absorbed and replaced by newly formed bone.

In this sense, the produced structures were characterized regarding roughness, wettability, β-TCP quantity and quality inside the structures after fabrication and the pH measured during cell culture (as consequence of β-TCP dissolution) and those aspects were correlated with cellular viability, distribution, morphology and proliferation.

These structures displayed a hydrophilic behavior and results showed that the addition of β-TCP to these cellular structures led to an alkalization of the medium, aspect that significantly influences the cellular response. Higher impregnation ratios were found more adequate for lowering the media pH and toxicity, and thus enhance cell adhesion and proliferation.

1. Introduction

Hip implants are currently used for restoring mobility in patients suffering from osteoarthritis or trauma, being implanted worldwide, per year, in one million people [1]. Currently hip implants are commonly made of Ti6Al4V alloy, due to this material excellent biocompatibility when in contact with body fluids, high strength (related with the addition of vanadium and aluminum) and corrosion resistance (due to the formation of an oxide layer) [2–6].

Typically, after 10 to 20 years of total hip arthroplasty surgery, revision surgeries are needed due to implant loosening [1,7] . The loss of the implant-bone fixation has been related to the stiffness mismatch existing between cortical bone and currently used hip implant materials [1,8]. In fact, current solutions are Ti6Al4V dense implants with an excessively high Young's modulus (≈ 110 GPa [2,9]) when compared to bone ($\approx 10–30$ GPa [2,9]). This mismatch causes a reduction on the

stress that is transferred from the implant to the cortical bone (stress-shielding effect), thus leading bone to resorb [1,2,8,10].

Although biocompatible, Ti6Al4V implants are bioinert, thus non-eliciting an enhanced biological interaction with the human body [11]. Ideally, for bone tissue repair it is important to find a nontoxic, biocompatible, bioactive solution owing suitable mechanical properties (stiffness and strength), that allow a free flow of nutrients to promote cell growth, proliferation and differentiation and consequently new tissue formation [12–14].

When scanning the available literature, different strategies are found, spanning different materials, combinations and structures. (i) Biomaterials like hydrogels are widely used for bone tissue repair once they promote a suitable environment highly similar to the extracellular matrix (ECM) for cell migration, adhesion, proliferation and adhesion. However, many challenges remain due to unsuitable mechanical and bioactive properties in natural and synthetic hydrogels, respectively

---

* Corresponding author.
  E-mail address: amafmcosta@gmail.com (M.M. Costa).

[13]. (ii) Bioactive ceramics (hydroxyapatite, β-Tricalcium Phosphate (β-TCP), bioactive glass [12,14]) are vastly studied for bone tissue repair due to its chemical composition highly similar to natural apatites of bone, however, its brittle nature make them not suitable for load bearing applications [12,14–17]. Many researchers overcome the lower mechanical properties of bioactive materials by introducing a second phase material. (iii) Low-dimensional nanomaterials (LDN), such as carbon nanotubes, graphene or boron nitride nanotubes are very promising reinforcements due to their ability to enhance these bioactive materials mechanical properties [14,18,19], especially suitable for fabricating scaffolds [18]. However, the use of LDN is still challenging once it is difficult to achieve their homogeneous dispersion, besides their low oxidation temperature, easily achieved when sintering the bioactive material [14,18,19]. (iv) Recent studies show the potential of using polymeric scaffolds with incorporation of bioactive ceramics or antibacterial agents [19,20], however their mechanical properties are still below these implants loading requirements [12]. (v) Regarding metallic alloys, there are some studies on bioactive reinforced composites for load-bearing applications with faster and enhanced osseointegration [3,17,21,22] while many studies address bioactive coatings for Ti6Al4V implants [9,23,24]. However, some problems arise when using coatings, especially the detachment of the coating layer, that may compromise the bioactive properties of the final implant and lead to local inflammatory reactions [21,22].

Considering the abovementioned strategies, a multi-material solution that gathers different materials appears as a promising solution towards the improvement of conventional hip implants by promoting multifunctionality. This study proposes a multi-material solution (Ti6Al4V and β-TCP) based on cellular structures that simultaneously lowers implant Young's modulus, add bioactivity, allow a flow of nutrients and waste while assuring bone ingrowth and vascularization [10,25]. Vascularization is extremely important in implants, especially after implantation, once it will potentiate a cascade of biological events that will resorb the damaged bone and replace it by newly formed bone [12,26].

This multifunctionality can be achieved by fabricating Ti6Al4V cellular structures impregnated with β-TCP bioactive ceramic that will be absorbed and replaced by newly formed bone. Selective Laser Melting (SLM) is an Additive Manufacturing technique that melts successive layers of metallic powders for building a final part [5,10,27,28] which allows an enormous freedom for designing cellular structures within the optimum pore size to enhance bone vascularization and ensuing bone ingrowth [25,29–31], reported between 100 and 400 μm [12,26,32].

Targeting hip implants, the present work shows the influence of these structures design on physical and chemical aspects that drive cellular response. The quantity and quality of the β-TCP inside the structures and the cell culture pH were evaluated and correlated with cellular viability, cellular distribution, morphology and proliferation on the surface and inside these structures.

2. Materials and methods

2.1. Specimens production

In this study, four different Ti6Al4V-based specimens were studied, being their details presented in Table 1.

The first group (G1) intends to replicate the material/surface condition usually found in several commercially available endosseous implants (hip, dental) [33,34] and in this sense will act as a control group. A Ti6Al4V casted/forged commercial rod with 6 mm diameter, purchased from Titanium Products (United Kingdom), was cut to obtain G1 specimens having 3 mm thickness. These specimens were then subjected to a sandblast-acid etching process (SLA) to achieve a microroughness of 2–4 μm (Ra), the most frequent value used in these implants [33]. This process begins by sand blasting the Ti6Al4V specimens

using spherical alumina particles (with a granulometric range between 106 and 150 μm) for 30 s followed by a 5 min acid-etching process (with 32% HCl, 96% H_2SO_4 and H_2O (2,1,1)) at 65 ± 3 °C. After etching the specimens were ultrasonically cleaned with isopropanol for 5 min.

The specimens from G2, G3 and G4 groups all start from Ti6Al4V cellular structure made by an additive manufacturing technology – Selective Laser Melting (SLM). The selection of this technology was due to its several advantages over conventional methods, in terms of cost, material waste, speed, reliability and accuracy [27,29,35]. These cellular structures were produced in a SLM equipment from SLM Solutions, model 125 HL. The powder used in the production was purchased from the equipment manufacturer (SLM Solutions GmbH, Germany). The processing parameters used for these structures fabrication were based in previous studies [5,36] being the laser power set as 90 W, a layer thickness of 30 μm and a scan speed and spacing of 600 mm/s and 80 μm, respectively. These cubic-like Ti6Al4V scaffolds have holes interconnected superiorly and also laterally and were designed to have an open-cell (pore) size of 400 μm and a wall thickness of 300 μm, having after production an average pore and wall sizes of 293 and 400 μm, respectively.

While G2 group represents the cellular structures obtained by SLM, G3 and G4 specimens incorporate β-TCP in these cellular structures, using different percentages of this bioactive (Table 1). The choice of alternative processes to AM to impregnate the bioactive material into these cellular structures is due to the fact that direct AM techniques of ceramic materials like β-TCP still pose some limitations due to the high temperatures involved in laser processing, leading to chemical degradation of the β-TCP, thus diminishing its bioactivity [37–39].

The specimens from G3 were prepared by immersing the cellular structures inside a viscous solution of β-TCP powder (Trans-Tech, Inc) and acetone (≈15% (w/v)) being then ultrasonically stirred. This solution was then heated under mechanical stirring to promote acetone evaporation. The β-TCP-Ti6Al4V scaffolds were then sintered, in a tubular furnace at 1100 °C for 2 h, under high vacuum, with a heating and cooling rate of 5 °C/min.

The fourth group of specimens (G4) was obtained using a powder metallurgy technique (Press and Sintering) for impregnating and afterwards sinter β-TCP inside the structures. After positioning the structures inside a steel mold, these were immersed in a β-TCP powder and acetone solution (≈63% (w/v)) and pressure was applied for 10 min using a hydraulic press, for injecting the bioactive to the open cells of the Ti6Al4V structures. These specimens were then removed from the mold and sintered in a tubular furnace at 1100 °C for 2 h, under high vacuum, with a heating and cooling rate of 5 °C/min.

The β-TCP percentage inside G3 and G4 specimens (named bioactive percentage) was obtained by weighting each sample before and after the impregnation process. This bioactive percentage was obtained dividing the mass of bioactive (determined by the mass difference before and after impregnation) by the final weight of the specimen. G3 group exhibited a bioactive percentage of 1.58 wt% while G4 exhibited 2.98 wt%.
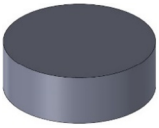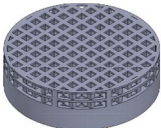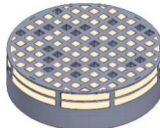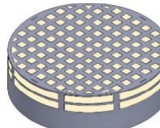
Besides this "bioactive percentage", an "impregnation ratio" was also determined by dividing the weighted mass of β-TCP inside the structures by the β-TCP mass that would totally fill the pores of the structures. The impregnation ratio of G3 and G4 was, therefore, 12.52% and 23.89%, respectively.

After production, G2, G3 and G4 specimens were polished using abrasive silicon carbide papers from mesh P120 till P4000 being afterwards ultrasonically cleaned with isopropanol for 5 min.

2.2. Specimens characterization

The produced specimens from the four groups were analyzed using Scanning Electron Microscopy (SEM) equipment (NanoSEM - FEI Nova 200 (FEG/SEM)). X-rays diffraction (XRD) analysis was conducted on cast Ti6Al4V (G1), Ti6Al4V cellular structures fabricated by SLM (G2)

Table 1
Groups detailed description.

Representation				
Group number	G1	G2	G3	G4
Description	Ti6Al4V Cast SLA treated	Ti6Al4V SLM	Ti6Al4V SLM β-TCP impregnated (1.58 wt%)	Ti6Al4V SLM β-TCP impregnated (2.98 wt%)

and Ti6Al4V cellular structures impregnated with β-TCP (G3 and G4). XRD's were collected using a 2Θ from 10 to 80° with a step size of 0.02 at 1 s per step, using a Bruker AXS D8 Discover equipment.

2.3. Surface roughness

The surface roughness of the specimens was assessed by using a contact profilometer (Surftest SJ 201from Mitutoyo, Tokyo, Japan). The test was conducted on the metallic walls of the structures using $\lambda_c = 0.8\,\mu m$, $\lambda_s = 2.5\,\mu m$, at 0.25 mm/s, according to ISO 4287-1997 [40]. From this test the average roughness (Ra), the peak-to-valley roughness (Rz) and the root-mean-square roughness of the departures of the profile from the mean line (Rq) were taken. For each sample, five measurements were performed to calculate average results. Surface roughness differences between the four groups were assessed by performing one-way ANOVA with *post hoc* Bonferroni multiple comparison test, where $p_{value} < 0.05$ was defined as statistical significant (GraphPad Prism v, GraphPad Software, La Jolla, California, USA).

2.4. Contact angle measurements

In order to determine the wettability properties of the metallic scaffolds, contact angle measurements for each group were performed by sessile drop technique using water and phosphate-buffered saline (PBS) as a probe liquid. The contact angle system OCA 15 plus (Dataphysics) was used to measure the angle formed by the droplets. Five droplets were measured for each group and the average was taken from these results. To assess the statistical difference between groups and among the two different solutions, two-way ANOVA and *post hoc* Bonferroni multiple comparison test was used (GraphPad Prism v, GraphPad Software, La Jolla, California, USA). For both statistical tests $p_{value} < 0.05$ was defined as statistical significant.

2.5. Cytotoxicity assessment

Short-term cytotoxicity tests were performed on the produced specimens following the protocol described by Silva et al. [41]. The scaffolds were incubated with minimum essential culture medium (MEM) and after each time-point (24 h, 7, 14, 21 and 28 days) the medium was extracted and filtered using a 0.45 mm pore-size filter. In all MEM tests, the material weight-to-extract fluid rate was constant at a rate of 0.2 g/ml. For this analysis, latex extracts with the same extraction protocol were used as positive controls for cell death and culture medium as negative control.

2.5.1. Cell culture

Rat lung fibroblasts L929 cell line from European Collection of Cell Cultures were cultured in 24-well plates (n = 3, 5×10^3 cells/well), and incubated in a humidified atmosphere with 5% CO_2 at 37 °C for 24 h. These cells were cultured in a Dulbecco's modified Eagle's culture medium (DMEM) supplemented with 10% fetal bovine serum (Gibco, Barcelona, Spain) and 1% antibiotic-antimycotic mixture (Sigma).

2.5.2. MEM extraction test

Cell culture medium was discarded from the wells 24 h after cell seeding. Subsequently, the MEM extraction fluid was added to the L929 cells. These cells were then incubated for another 72 h at 37 °C. The incubation was placed in a humidified atmosphere with 5% CO_2. Live/death assay was conducted by staining live cells with calcein-AM (1 mg/ml; Molecular Probes, Eugene, OR) and nonviable cells with propidium iodide (0.1 mg/ml; Molecular Probes). After staining, cultures were then observed under a fluorescence microscope (BX-61; Olympus, Hamburg, Germany).

Statistical analysis was performed by using one-way ANOVA using post-hoc Bonferroni to assess the statistical significant differences on live/death results between all the produced specimens under study ($p_{value} < 0.05$ was defined as statistical significance).

Additionally, pH values of the medium of each group were also determine by means of inoLab pH 720 (WTW, Germany) pH meter to assess its variance on the specimens leachables.

2.6. Direct contact assay

Direct contact assay was used to assess *in vitro* biocompatibility of the scaffolds by evaluating cell attachment and proliferation of human mesenchymal stem cells (hMSCs) [42]. These hMSCs were derived from human bone marrow, purchased on Lonza (Switzerland) and were cultured as monolayers in Alpha MEM medium supplemented, in sterile T175 tissue culture flasks, with 10% FBS and 1% antibiotic-antimycotic mixture.

Moreover, the same protocol was used to assess cell seeding [43]. Briefly, the P6 hMSCs were trypsinized, centrifuged and resuspended in α -MEM medium. Subsequently, 50 µl of medium containing 1×10^5 cells were seeded during one hour on top of the scaffold. After seeding, 750 µl of culture medium was added to each well and cell-scaffolds were incubated in a humidified atmosphere at 37 °C, containing 5% CO_2, for 3 and 7 days, with medium changes every 3 days.

2.6.1. Cell distribution, morphology and proliferation

After each timepoint (3 and 7 days), hMSCs distribution and morphology were assessed through a *phalloidin/DAPI* staining [44], in which the phalloidin and *DAPI* (4′,6-diamidino-2-phenylindole) stained cytoskeleton (red) and nucleus (blue), respectively. Cells were fixed with paraformaldehyde 4% for 30 min at room temperature and, subsequently, the cell-scaffold structure was washed and sliced to evaluate cell maintenance and migration throughout the scaffold. The top and the cross-section images of the scaffold were incubated with 0.1 µg/ml of *phalloidin* (Sigma) and 1 µg/ml of *DAPI* for 30 min. Lastly, the cell-scaffolds structures were washed with PBS and observed using a confocal microscope (Fluoview FV 1000; Olympus, Hamburg, Germany).

3. Results and discussion

3.1. Microstructural characterization

SEM micrographs of the produced specimens (G1–G4) can be observed in Fig. 1. Group G1 was included as control group, once it
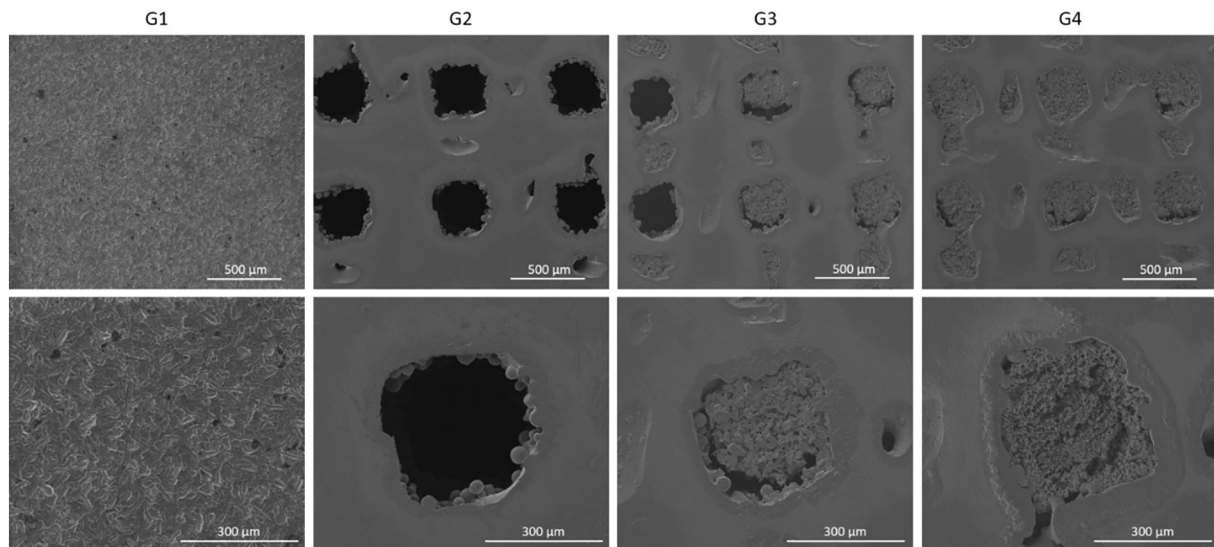
Fig. 1. SEM micrographs of commercial Ti6Al4V sample (G1), SLM processed Ti6Al4V structures (G2), and Ti6Al4V SLM structures impregnated with β-TCP with a bioactive percentage of 1.58 wt% (G3) and 2.98 wt% (G4).

represents the typical surface topography present in the majority of commercial hip implants. This topography results from the SLA process, as previously mentioned in the experimental section.

The micrographs from G2, G3 and G4 depicted in Fig. 1 prove that the production by SLM of these Ti6Al4V cubic-like cellular structures was successfully accomplished. As seen in Fig. 1 it is possible to observe the scaffold structure (holes and walls) evidencing a high densification of the material, proving that SLM process is suitable for the fabrication of these structures.

Additionally, the micrographs of G3 and G4 structures show that G4 attained a higher impregnation ratio than G3. These evidences are in accordance with the calculated bioactive percentages, of 1.58 wt% for G3 and 2.98 wt% for G4.

XRD analysis was performed in specimens from all the groups to assess the influence of the production process on the crystalline structure of the alloy (Ti6Al4V) and on the condition of the bioactive material inside the cellular structure.

Fig. 2 presents a XRD spectrum for each group, with the respective microstructures being displayed in Fig. 3. It is possible to detect from all spectra the hexagonal close-packed (HCP) and body-centered cubic (BCC) crystalline structures of titanium. By comparing G1 and G2 XRD patterns, no significant differences were found. From Fig. 3, it is possible to observe the microstructure of G1 which corresponds to Ti6Al4V cast material, being visible the α grains at light gray and β phase in dark gray. This microstructure is commonly found reported in literature for Ti6Al4V specimens produced by casting [45,46].

Some studies already reported that Ti6Al4V produced by SLM present some microstructural differences from the cast alloy [6,45]. SLM process is characterized by a fast cooling rate, which will influence the microstructure of Ti6Al4V by increasing the needle-shape β phase [47]. In fact, SLM fast cooling rate will promote a transformation from β-phase to martensitic α′ phase [36]. From the XRD pattern of G2 (SLM Ti6Al4V cellular structure) it is not possible to distinguish the α′ from the α phase once both are characterized by the same hexagonal close packed crystalline structure [45,48]. However, from Fig. 3, G2 microstructure evidences the presence of martensitic α′ phase, as also proven in other studies [45,47].

The addition of β-TCP to the scaffolds (G3 and G4) led to the presence of a new peak near 30–35° on the XRD pattern, corresponding to β-TCP phase. G3 and G4 microstructure (Fig. 3) suggests that the sintering process of β-TCP could act as a heat treatment for Ti6Al4V once the temperatures involved in this process are quite high. This

phenomenon, according to literature, will lead to the formation of β-phase that results from the decomposition of martensite phase at high temperatures (above β transus) [49], which is in accordance with the typical β-phase microstructure found on G3 and G4 (Fig. 3).

3.2. Roughness

Despite the high number of parameters conditioning cell adhesion and proliferation, surface energy appears to be a dominant factor [50]. The surface energy depends on the surface charge, microstructural topography and chemical composition [51]. Surface roughness can modulate the activity of cells interacting with an implant [52] and therefore strongly disturb the relationship between surface energy and cell proliferation [50]. In this sense, the surface of an implant significantly affects the implant-cell interactions [50].

Surface roughness values (Ra, Rz and Rq) of all groups are presented in Table 2, being the results for Ra statistically analyzed in Fig. 4.

As seen in Table 2, G1 that corresponds to cast Ti6Al4V SLA treated presents a roughness value of $1.90 \pm 0.10\,\mu m$. This value is very similar to those found in literature for this treatment on this material [53]. Furthermore, studies reveal that in acid etched specimens a hydrogen desorption occurs, consequently leading to the formation of a titanium hydride (TiH_2) that will also lead to increased roughness [54]. The roughness promoted on this group represents the commercial solution found in implants. According to the statistical analysis presented on Fig. 4, G2, G3 and G4 groups are statistically different comparing to G1 group (representing the commercial solution).

The Ti6Al4V cellular structures, as-produced by SLM, present a typical rough surface due to the partial melting of powders on the vicinity of the laser path [5,11]. The as-produced cellular structures produced in this study revealed a roughness of $19.75 \pm 1.50\,\mu m$ (Ra). Those values are aligned with literature, where Ti6Al4V specimens produced by SLM display an as-produced roughness (before polishing) of $17.60 \pm 3.70\,\mu m$ [55]. Ponsonnet et al. [50] reported that a roughness value lower than 1 μm favors cell proliferation, regardless of the wettability of the specimens. For this reason, as mentioned in the experimental section, G2, G3 and G4 were polished to reduce this as-produced roughness. The SLM Ti6Al4V cellular structures (G2) displayed an Ra of $0.18 \pm 0.04\,\mu m$, while G3 and G4 groups present a slight tendency to display lower values when compared with G2. This could be explained by the presence of surface defects, inherent of the SLM process, which as clearly seen in Fig. 5, will contribute to a higher roughness on the
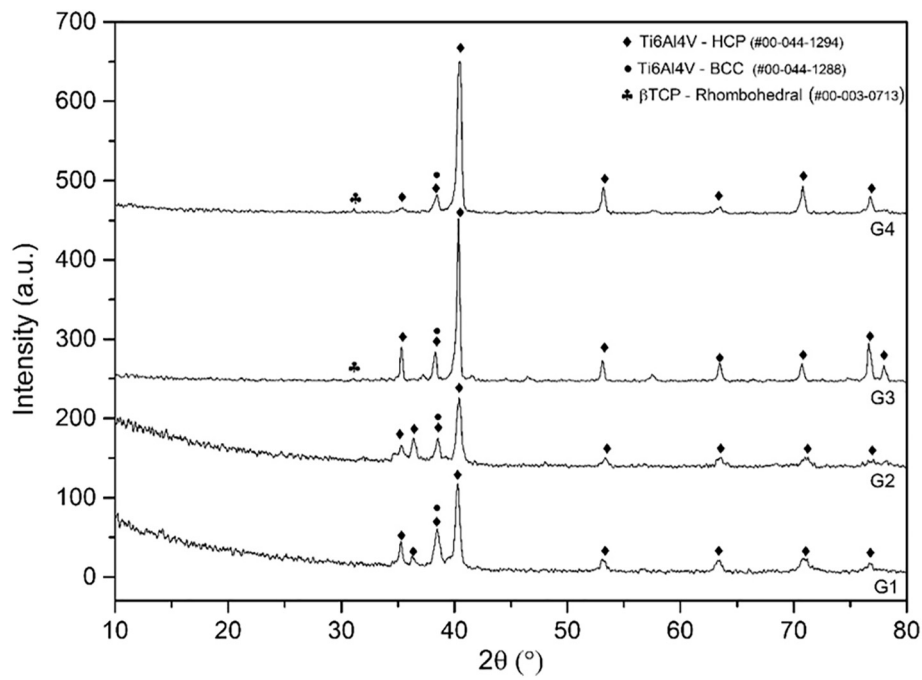
Fig. 2. XRD patterns of commercial Ti6Al4V sample (G1), SLM processed Ti6Al4V structures (G2) and Ti6Al4V SLM structures impregnated with β-TCP with a bioactive percentage of 1.58 wt% (G3) and 2.98 wt% (G4).
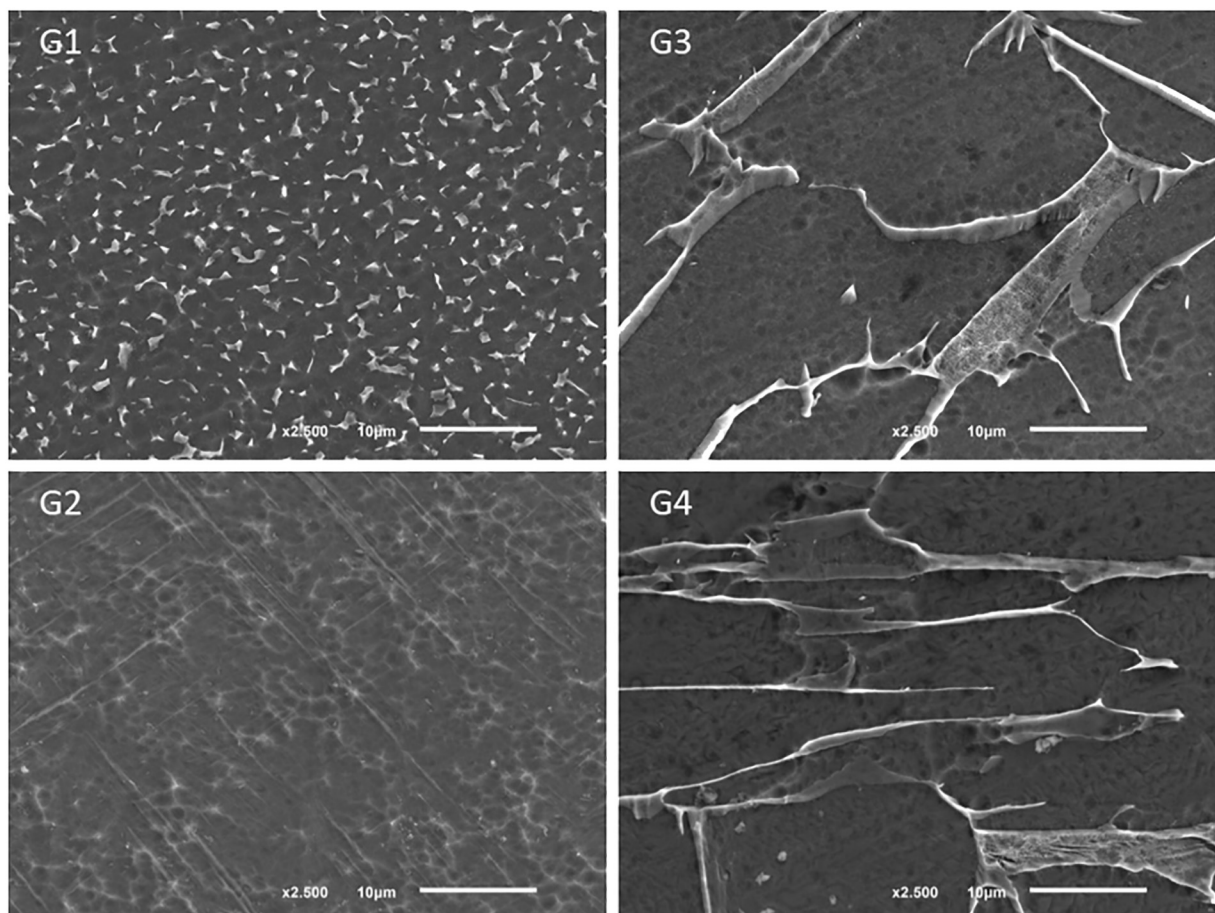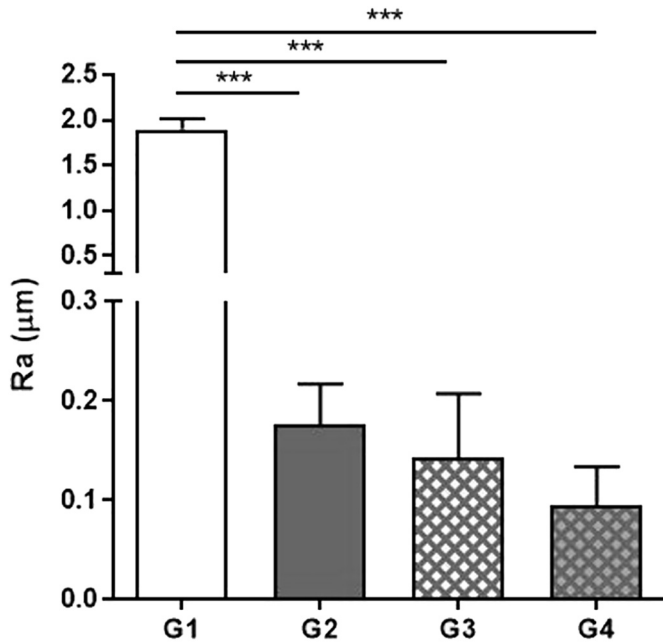

Fig. 3. Ti6Al4V microstructure for the produced groups (G1–G4) after acid etching, acquired by SEM.

Table 2
Roughness measurements of the four groups.

Group	Ra (µm)	Rz (µm)	Rq (µm)
G1	1.90 ± 0.10	14.17 ± 0.99	2.38 ± 0.09
G2	0.18 ± 0.04	2.13 ± 1.22	0.29 ± 0.13
G3	0.14 ± 0.06	1.24 ± 0.6	0.21 ± 0.12
G4	0.10 ± 0.03	0.67 ± 0.14	0.12 ± 0.04

Table 3
Water and PBS contact angles (mean ± SD) of Ti6Al4V Cast, Ti6Al4V SLM structures, and Ti6Al4V impregnated structures with 1.58 wt% and 2.98 wt. of β-TCP.

Group	Contact angle (average ± SD (°))	
	Water	PBS
G1	97.76 ± 3.02	92.90 ± 4.09
G2	Undetectable	Undetectable
G3	46.04 ± 6.45	46.80 ± 3.86
G4	20.92 ± 2.23	18.50 ± 2.52

Fig. 4. Surface roughness values (Ra) for all groups. Data are presented as average ± SD (n = 5). Symbol *** denote statistically significant differences ($p < 0.001$) in comparison with G1.

metallic walls (especially on G2). However, the impregnation process will promote a filling of those defects with bioactive materials (see G3 and G4 in Fig. 5), which will, consequently, diminish the roughness.

3.3. Wettability

Wettability was assessed for all the produced specimens in order to understand its influence on cell adhesion. It is known that the surface chemical composition and charge affect the wettability of the material and therefore influence the interaction between tissue and implant and consequently osseointegration [50,56,57] When interacting with biological fluids, highly hydrophilic surfaces are preferred rather than hydrophobic ones, once, when implanted in bone, hydrophilicity

surfaces lead to an increased bone formation [56,57]. A surface is considered hydrophilic when the contact angle is approximate or lower than 65° [58].

The wettability of each scaffold was assessed by measuring the contact angle at the moment the drop touched the surface.

The as-produced Ti6Al4V SLM-fabricated scaffolds (having a Ra of 19.75 ± 1.50 µm) displayed water and PBS contact angles of 129.46 ± 5.00° and 120.78 ± 2.81°, respectively, thus being considered non-suitable for cell interaction, once their surface is highly hydrophobic. This aspect reinforced the need to polish the cellular structures (either impregnated or not) from groups G2, G3 and G4.

Two different fluids were used for these wettability tests: water in order to be comparable with results found in literature for similar specimens and PBS once it is more representative of a biological fluid. The water and PBS contact angles that were measured are presented on Table 3 and Fig. 6 depicts the statistical results regarding the impregnated groups, G3 and G4, in water and PBS.

From Table 3 it is possible to conclude that from all the produced groups, G1 is the one that displays the most hydrophobic behavior (recalling that this group corresponds to SLA cast Ti6Al4V). These contact angles are in good agreement with available values found in literature [53]. In fact, this hydrophobic behavior has been reported as a consequence of forming TiH_2 on the material's surface, due to hydrogen desorption [54], as proven in several studies regarding SLA-treated specimens where this titanium hydride was found [54,59]. Furthermore, wetting properties are influenced by roughness, and according to Wenzel model [60], surface roughness will enhance liquid repellence when the contact angle is higher than 90° while surface roughness will promote liquid spreading for contact angle below 90° [60]. The former situation (contact angle higher than 90°) occurs in specimens from group G1, where the highest roughness is found.

All the SLM produced specimens presented hydrophilic surfaces since the measured contact angles are lower than 65° [58]. When comparing the results obtained using water and those using PBS, no significant differences regarding the contact angle were found. In porous structures such as Ti6Al4V SLM-cellular structures from G2, if the pressure is enough, the water will pass through the pores [60]. In
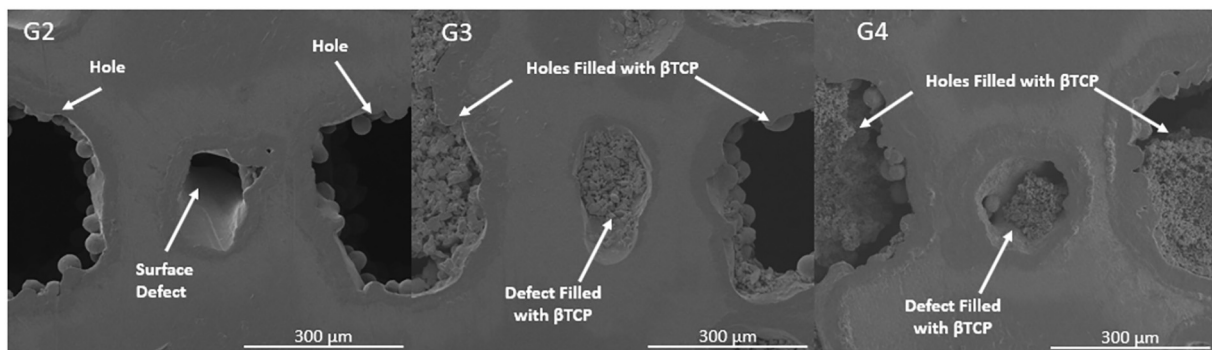
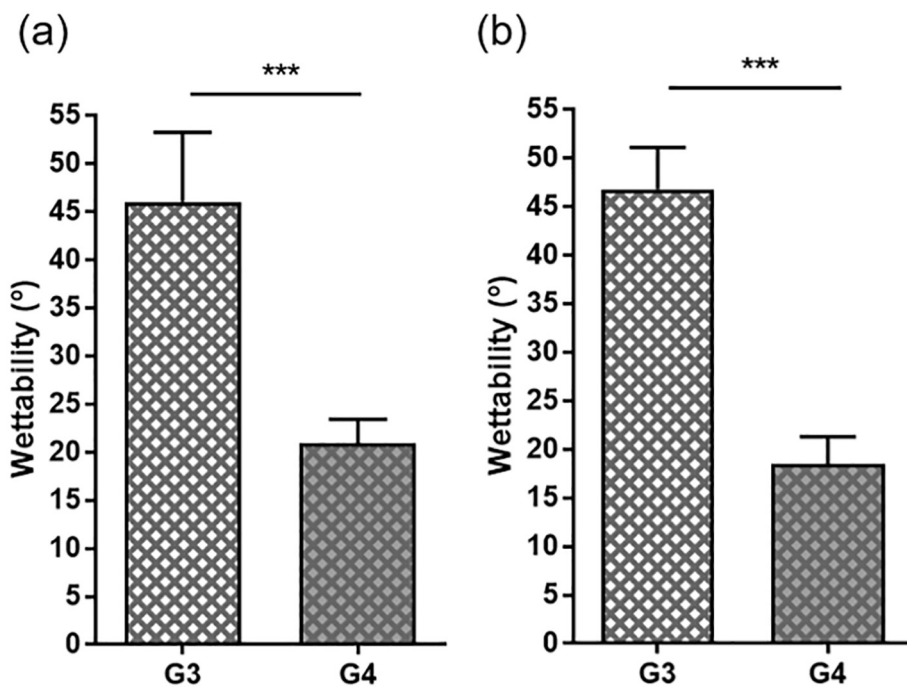**Fig. 5.** SLM structures surface defects.

Fig. 6. - Differences between G3 and G4 for (a) water and (b) PBS contact angles. Data are presented as average ± SD (n = 5). Symbol *** denotes statistically significant differences ($p < 0.001$) between both groups.
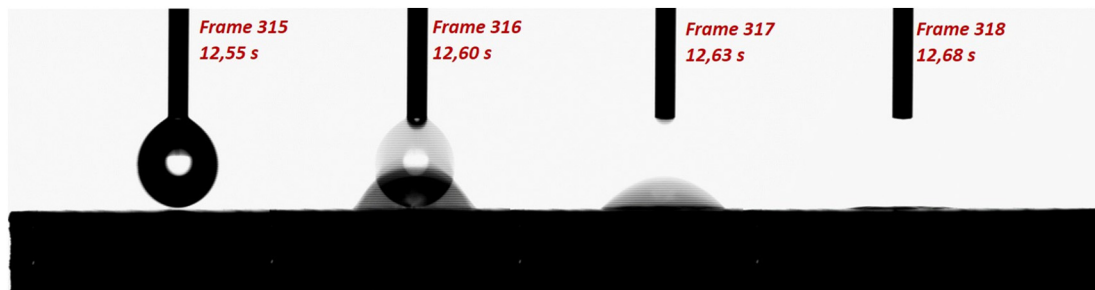

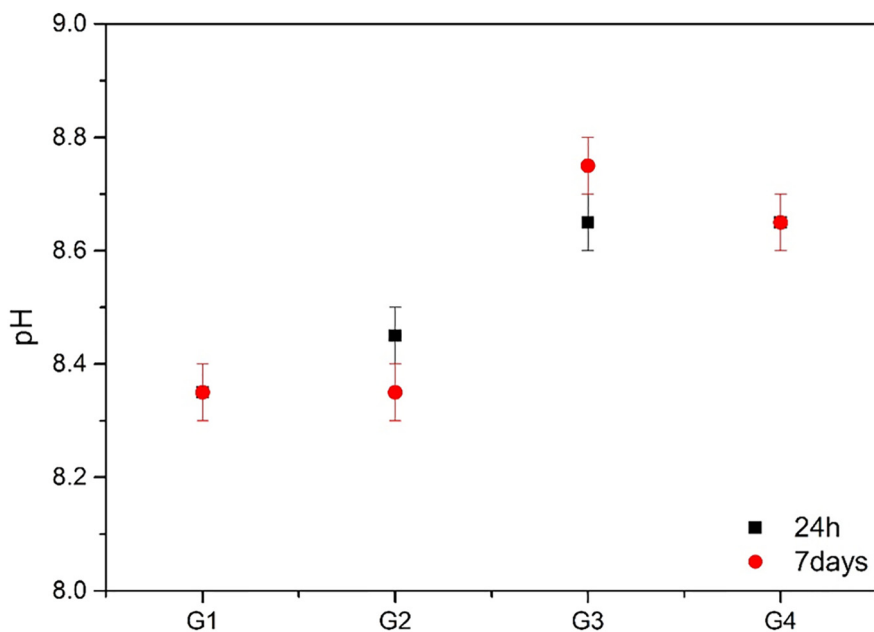**Fig. 7.** Hydrophilic behavior of Ti6Al4V SLM cellular structures (G2).

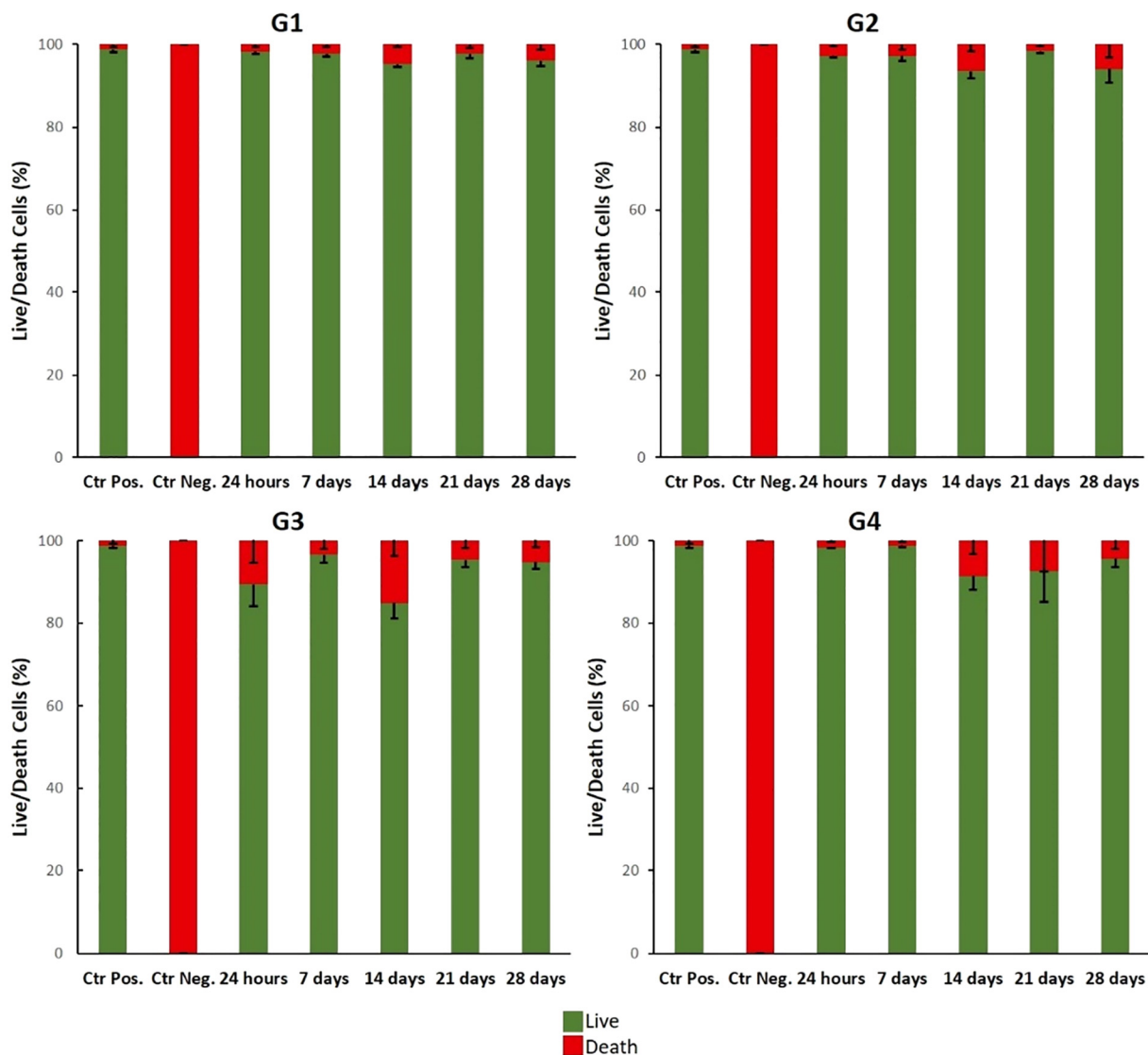**Fig. 8.** pH results for all the groups after 24 h and 7 days.

Fig. 9. Cell viability of L929 cells after culturing with the four groups of scaffolds for 24 h, 7, 14, 21 and 28 days.

this group of specimens, it is not possible to measure a static contact angle right after the drop gets in contact with the specimen, as seen in the frame sequence presented in Fig. 7. The design of this specimen, *i.e.* the open cell geometry together with the low surface roughness contribute to this super hydrophilic behavior once both water and PBS drops spread very quickly on its surface and throughout the specimens' porosity.

Another model that correlates surface roughness with wetting properties is Cassie-Baxter model [61]. In this model, air bubbles trapped between the liquid drop and the surface are also a factor that affects wettability [61]. In G2 group the interconnected pores will increase the contact area between the liquid and the solid and, consequently, the capillary forces. When the pressure of the air bubbles trapped inside the pores is overcame by these capillary forces, the capillary-pressure balance for these structures is disrupted and will eliminate this air pressure effect [62]. This behavior was clearly seen in G2 group, with water and PBS spreading inside the structure.

According to literature, hydrophilicity is preferable over hydrophobicity once it allows protein adsorption at an implant surface and consequently lead to an enhanced interaction between cells and the surface [56,57].

Groups G3 and G4 also display a hydrophilic behavior, with higher contact angles than that of G2. For G3 and G4, statistical results (two-

way ANOVA) revealed no significant differences on wettability when regarding the solution (water *versus* PBS). On the other hand, significant statistical differences between G3 and G4 wettability were found, either for water and PBS solution (Fig. 6), with lower contact angles being consistently measured for G4.

G4 lower average contact angle when compared with G3, could be related with the higher impregnation ratio in G4. Being β-TCP a hydrophilic material [63], the higher the quantity of this bioactive material, the higher the hydrophilicity of the specimen. Additionally, it is important to highlight that the effect of the capillary forces described for G2, also applies to the structures from G3 and G4 groups, once for both groups a full impregnation is not promoted.

3.4. pH

The biodegradation of biomaterials like calcium phosphates is a combination of physical, chemical and biological factors [64]. The dissolution of β-TCP leads to an increase on the concentration of Ca^{2+} and PO_4^{3-} in the medium, as shown in the following Eq. (1) [65]:

$$Ca_3(PO4)_2 \rightarrow Ca^{2+} + PO_4^{3-} \tag{1}$$

$$PO_4^{3-} + H^+ \rightarrow HPO_4^{2-} \tag{2}$$
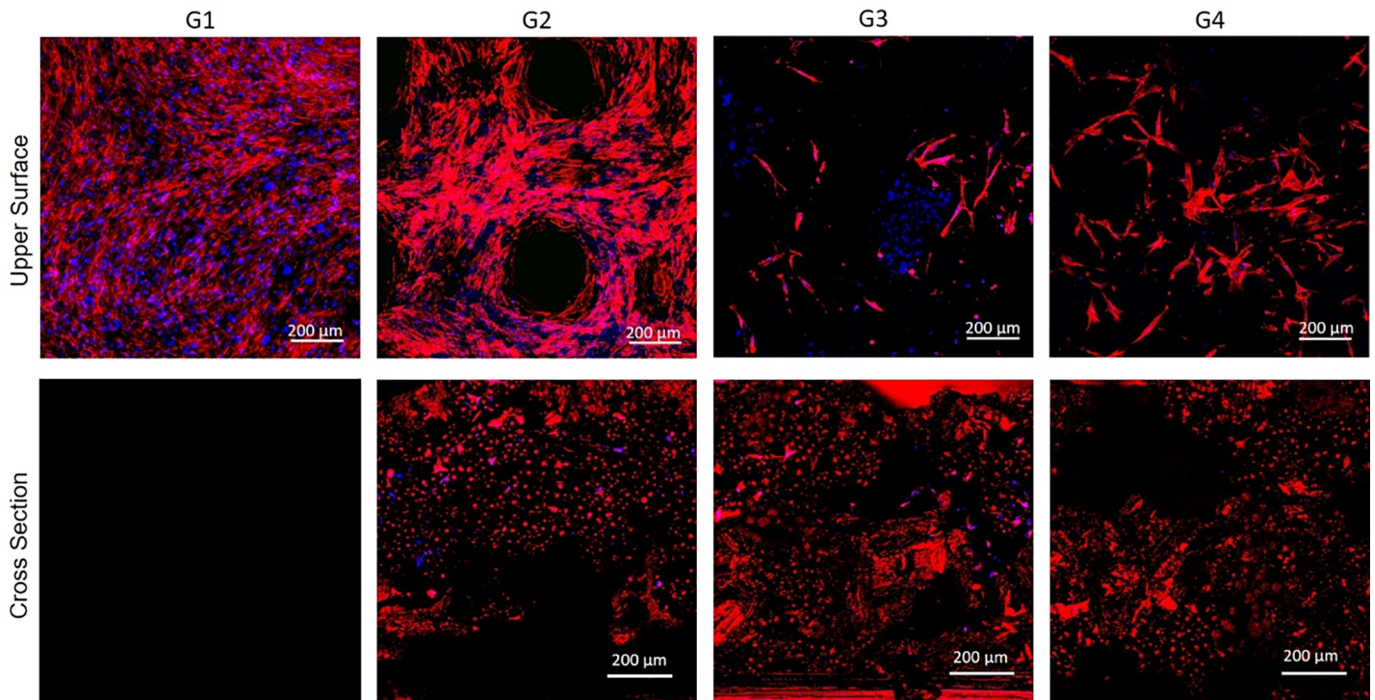
Fig. 10. Fluorescence microscopy images of hMSC cultured for 7 days on commercial Ti6Al4V (G1), SLM Ti6Al4V structures (G2), and Ti6Al4V SLM structures impregnated with β-TCP with a bioactive percentage of 1.58 wt% (G3) and 2.98 wt% (G4). hMSCs were stained with *DAPI* (nucleus at blue) and with *phalloidin* (actin cytoskeleton at red). Images on the top are from the top surface whereas cross section images are on the bottom. (For interpretation of the references to color in this figure legend, the reader is referred to the web version of this article.)
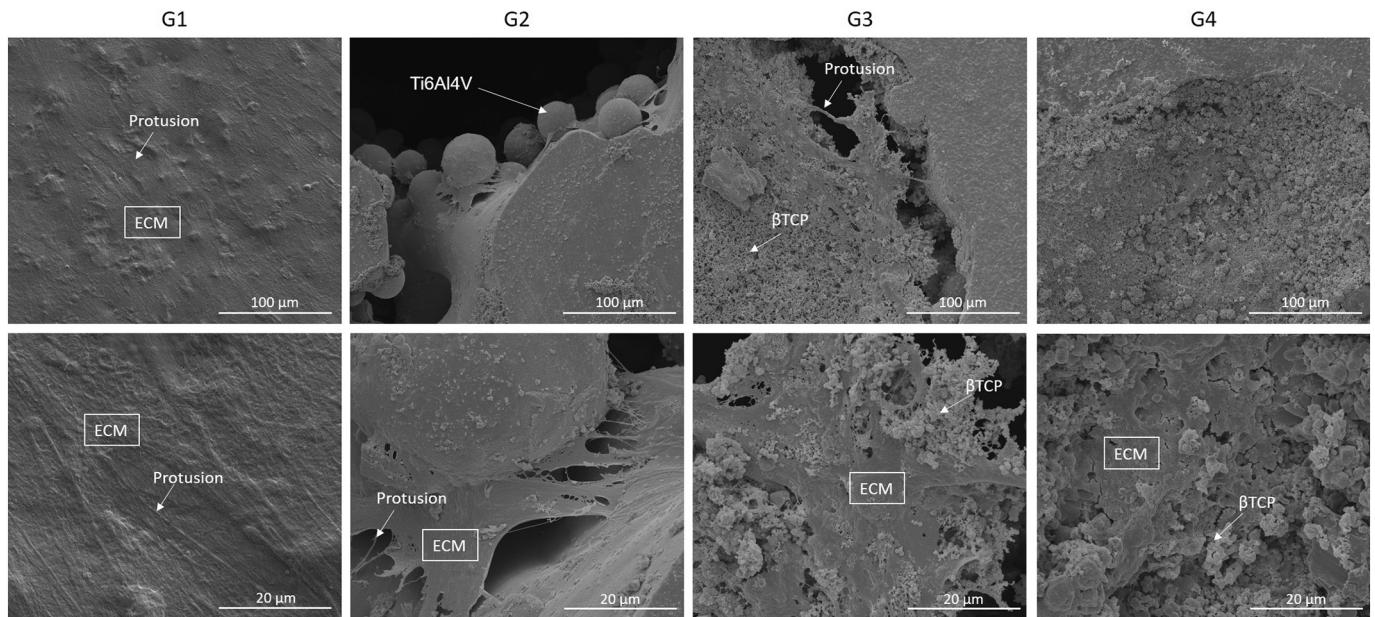
Fig. 11. SEM micrographs of hMSC, after an incubation of 7 days, cultured on commercial Ti6Al4V sample (G1), SLM processed Ti6Al4V structures (G2), and Ti6Al4V SLM structures impregnated with β-TCP with a bioactive percentage of 1.58 wt% (G3) and 2.98 wt% (G4).

Subsequently, PO_4^{3-} ions will react with H^+ ions, according to Eq. (2), leading to an alkalization of the medium [65,66]. This outcome has been reported in several studies found in literature [65]. Although cellular and phagocytic activities and also cell mediated factors tend to decrease the pH of the surrounding medium [64], this acidification is not enough to compensate pH increase induced by the dissolution of β-TCP. This alkalization has a profound impact in hMSC's proliferation and consequent osteogenic differentiation [67]. Moreover, the extended release of calcium ions into the medium promotes the inflow of calcium

ions in osteoblasts, which slightly hyperpolarizes the plasma membrane and thus stimulates osteoblast ATP (adenosine triphosphate) production [68].

Fig. 8 depicts the effect of the specimens' leachables in the pH measured at two different culture timepoints: 24 h and 7 days. These results show that G3 group was the one that displayed the higher pH, for both timepoints, corresponding to the leachables with a more alkaline media. On the other hand, the group that displays a more acidic solution is the commercial solution (group G1), with similar pH being
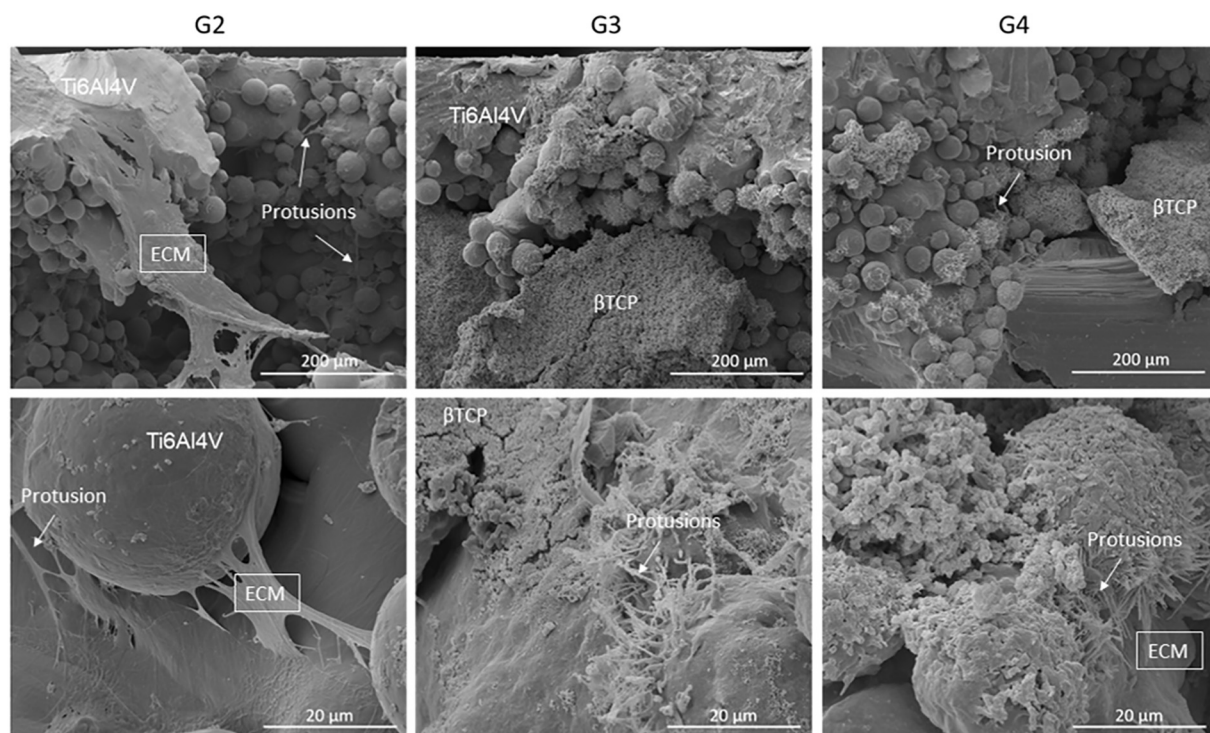
Fig. 12. SEM cross section micrographs of hMSC, after 7 days of incubation, SLM processed Ti6Al4V structures (G2), and Ti6Al4V SLM structures impregnated with β-TCP with a bioactive percentage of 1.58 wt% (G3) and 2.98 wt% (G4).

found for both timepoints.

For G3 and G4 specimens, the porosity filled with β-TCP will hamper the free flow of the solution throughout the interconnected holes and, therefore, increase the pH inside the structures (Fig. 8). This pH increase is more pronounced in G3 group, due to G3 lower impregnation ratio (when compared to G4). Due to this lower impregnation, G3 specimens have a higher contact area between the bioactive material and the medium. As a consequence, a higher dissolution rate occurs, thus increasing the pH.

3.5. Cell viability

The cytotoxicity of the produced specimens was assessed in order to ascertain the toxic effect of the products released from the metallic scaffolds during incubation with MEM. Fig. 9 shows the viability results for the four groups in five different timepoints. Moreover, a statistical analysis was performed to compare these results. No significant differences were observed between groups, even for the higher timepoint of MEM extraction (28 days). Overall, we can assume that all constructs were not releasing toxic substances to the medium, proving that these specimens assure a suitable environment for cells to proliferate and attach. However, at the 14 days extraction, the medium of G3 scaffolds seems to indicate some levels of toxicity, that can be related to the lack of medium renewal inside the pores. Nonetheless, this effect is not found on the ensuing timepoints.

3.6. Cell adhesion

One of the factors that influence cell adhesion is the surface energy, which depends on the chemical composition, charge and microstructural topography of the surface [15]. On metallic materials, cell adhesion increases linearly with surface hydrophilicity and thus surface energy has a direct effect on the cellular adhesion strength [51]. Fig. 10 shows the cell adhesion on the surface (top images) and inside the Ti6Al4V-based structures (bottom images), after an incubation of 7 days. Both G1 and G2 groups show a densely and uniform cell

distribution on the surface and, in the case of G2, cells seem to easily penetrate the scaffold. After an incubation of 7 days, the cell adhesion on the surface of the cellular structures impregnated with β-TCP (G3 and G4) is lower, compared with the one without bioactive material (G2), although being possible to identify cells inside the G3 and G4 scaffolds. For these two groups, cells have a spindle shape and, while on the constructs with lower impregnation ratio (G3) *DAPI* stained cell nucleus are observed on the bioactive location, this stain is not abundantly present on G4 scaffolds (with higher impregnation ratio).

The morphology of hMSC after incubation for 7 days was assessed by SEM (Figs. 11 and 12). Generally, all the groups exhibited cell protrusions and the formation of extracellular matrix (ECM) after 7 days of incubation. Fig. 11 shows that cells are well distributed on the surface of specimens from G1 group, proving that G1 sandblasted and acid-etched (SLA) surface is effective for superficial cell growth. On the other hand, scaffolds allow the ingrowth of cells, to enable future osseointegration of metallic implants owing this structure. The cellular structures produced by SLM (G2) show that this topography and roughness are adequate for cell culture, once several cells protrusions are observed in Fig. 11 (surface) and Fig. 12 (cross-section). For β-TCP impregnated scaffolds (G3 and G4), cells display a flattened morphology, with protrusions being less visible, when compared to the SLM constructs without bioactive (G2), for both surface and cross section.

These results show that the presence of β-TCP inside these cellular structures influences the pH of the medium, that in turn will affect cell viability. In this sense, a higher impregnation ratio is preferable, once it will lead to a lower pH and toxicity and, consequently, enhanced cell adhesion and proliferation.

4. Conclusions

This study proposes a solution for load-bearing implants by designing a multi-material Ti6Al4V cellular structure impregnated with β-TCP. This multi-material structures were designed to be the outer layer of a hip implant that assures no bioactive detachment upon implantation and allow cell adhesion and proliferation not only on implant

surface but also inside the structure. The processing route used for manufacturing these multi-material structures (combining an additive manufacturing technique (SLM) with Press and Sintering) allowed the fabrication of a load-bearing interconnected structure that allows bone ingrowth, vascularization and flow of nutrients, and on the other hand assured the bioactive retention and non-degradation within the Ti6Al4V cellular structure. The influence of the design on some of the physical and chemical properties was evaluated. All the produced cellular structures revealed a hydrophilic behavior when compared with the commercial solution due to its interconnected porosity. Results revealed that when adding β-TCP to these structures, although nontoxic, the medium becomes more alkaline. Furthermore, the β-TCP quantity inside the structures had a direct influence on the pH of the medium, affecting significantly cells behavior. In this context higher impregnation ratios were found more adequate in these structures, for lowering the medium pH and promoting cell adhesion and proliferation. This solution can also be used to incorporate drugs into metallic cellular structures and therefore create a drug delivery system to treat, for instance, local infections.

Acknowledgments

References

[1] U. Holzwarth, G. Cotogno, Total hip arthroplasty - state of the art, Chall. Prospects (2012), https://doi.org/10.2788/31286.

[2] Q. Chen, G.A. Thouas, Metallic implant biomaterials, Mater. Sci. Eng. R. Rep. 87 (2015) 1–57, https://doi.org/10.1016/j.mser.2014.10.001.

[3] T.A. Dantas, C.S. Abreu, M.M. Costa, G. Miranda, F.S. Silva, N. Dourado, J.R. Gomes, Bioactive materials driven primary stability on titanium biocomposites, Mater. Sci. Eng. C 77 (2017) 1104–1110, https://doi.org/10.1016/j.msec.2017.04.014.

[4] S. Bruschi, R. Bertolini, A. Ghiotti, Coupling machining and heat treatment to enhance the wear behaviour of an additive manufactured Ti6Al4V titanium alloy, Tribol. Int. 116 (2017) 58–68, https://doi.org/10.1016/j.triboint.2017.07.004.

[5] F. Bartolomeu, M. Sampaio, O. Carvalho, E. Pinto, N. Alves, J.R. Gomes, F.S. Silva, G. Miranda, Tribological behavior of Ti6Al4V cellular structures produced by selective laser melting, J. Mech. Behav. Biomed. Mater. 69 (2017) 128–134, https://doi.org/10.1016/j.jmbbm.2017.01.004.

[6] F. Bartolomeu, M. Buciumeanu, M.M. Costa, M. Gasik, F.S. Silva, G. Miranda, Multi-material Ti6Al4V & PEEK cellular structures produced by selective laser melting and hot pressing: a tribocorrosion study targeting orthopedic applications, J. Mech. Behav. Biomed. Mater. 89 (2018) 54–64, https://doi.org/10.1016/j.jmbbm.2018.09.009.

[7] F. Bartolomeu, C.S. Abreu, C.G. Moura, M.M. Costa, N. Alves, F.S. Silva, G. Miranda, Ti6Al4V-PEEK multi-material structures – design, fabrication and tribological characterization focused on orthopedic implants, Tribol. Int. 131 (2018) 672–678, https://doi.org/10.1016/j.triboint.2018.11.017.

[8] S. Affatato, Perspectives in Total Hip Arthroplasty - Advances in Biomaterials and Their Tribological Interactions, Woodhead P, 2014, https://doi.org/10.1016/B978-1-78242-031-6.50016-7.

[9] D. Apostu, O. Lucaciu, C. Berce, D. Lucaciu, D. Cosma, Current methods of preventing aseptic loosening and improving osseointegration of titanium implants in cementless total hip arthroplasty: a review, J. Int. Med. Res. (2017), https://doi.org/10.1177/0300060517732697 (030006051773269).

[10] X.P. Tan, Y.J. Tan, C.S.L. Chow, S.B. Tor, W.Y. Yeong, Metallic powder-bed based 3D printing of cellular scaffolds for orthopaedic implants: a state-of-the-art review on manufacturing, topological design, mechanical properties and biocompatibility, Mater. Sci. Eng. C 76 (2017) 1328–1343, https://doi.org/10.1016/J.MSEC.2017.02.094.

[11] N. Taniguchi, S. Fujibayashi, M. Takemoto, K. Sasaki, B. Otsuki, T. Nakamura, T. Matsushita, T. Kokubo, S. Matsuda, Effect of pore size on bone ingrowth into porous titanium implants fabricated by additive manufacturing: an in vivo experiment, Mater. Sci. Eng. C 59 (2016) 690–701, https://doi.org/10.1016/j.msec.2015.

[12] C. Gao, S. Peng, P. Feng, C. Shuai, Bone biomaterials and interactions with stem cells, Bone Res. 5 (2017) 1–33, https://doi.org/10.1038/boneres.2017.59.

[13] M. Liu, X. Zeng, C. Ma, H. Yi, Z. Ali, X. Mou, S. Li, Y. Deng, N. He, Injectable hydrogels for cartilage and bone tissue engineering, Bone Res. 5 (2017) 1–25, https://doi.org/10.1016/j.actbio.2017.01.036.

[14] C. Gao, P. Feng, S. Peng, C. Shuai, Carbon nanotube, graphene and boron nitride nanotube reinforced bioactive ceramics for bone repair, Acta Biomater. 61 (2017) 1–20, https://doi.org/10.1016/j.actbio.2017.05.020.

[15] D.H. Lee, N. Tripathy, J.H. Shin, J.E. Song, J.G. Cha, K.D. Min, C.H. Park, G. Khang, Enhanced osteogenesis of β-tricalcium phosphate reinforced silk fibroin scaffold for bone tissue biofabrication, Int. J. Biol. Macromol. 95 (2017) 14–23, https://doi.org/10.1016/j.ijbiomac.2016.11.002.

[16] B. Li, Z. Liu, J. Yang, Z. Yi, W. Xiao, X. Liu, X. Yang, W. Xu, X. Liao, Preparation of bioactive β-tricalcium phosphate microspheres as bone graft substitute materials, Mater. Sci. Eng. C 70 (2017) 1200–1205, https://doi.org/10.1016/j.msec.2016.03.040.

[17] T.A. Dantas, M.M. Costa, G. Miranda, F.S. Silva, C.S. Abreu, J.R. Gomes, Effect of HAp and β-TCP incorporation on the tribological response of Ti6Al4V biocomposites for implant parts, J. Biomed. Mater. Res. - Part B Appl. Biomater. (2017) 1–7, https://doi.org/10.1002/jbm.b.33908.

[18] C. Shuai, P. Feng, P. Wu, Y. Liu, X. Liu, D. Lai, C. Gao, S. Peng, A combined nanostructure constructed by graphene and boron nitride nanotubes reinforces ceramic scaffolds, Chem. Eng. J. 313 (2017) 487–497, https://doi.org/10.1016/j.cej.2016.11.095.

[19] C. Shuai, W. Guo, P. Wu, W. Yang, S. Hu, Y. Xia, P. Feng, A graphene oxide-Ag co-dispersing nanosystem: dual synergistic effects on antibacterial activities and mechanical properties of polymer scaffolds, Chem. Eng. J. 347 (2018) 322–333, https://doi.org/10.1016/j.cej.2018.04.092.

[20] P. Feng, P. Wu, C. Gao, Y. Yang, W. Guo, W. Yang, C. Shuai, A Multimaterial Scaffold, With tunable properties: toward bone tissue repair, Adv. Sci. 5 (2018) 1–15, https://doi.org/10.1002/advs.201700817.

[21] G. Miranda, A. Araújo, F. Bartolomeu, M. Buciumeanu, O. Carvalho, J.C.M. Souza, F.S. Silva, B. Henriques, Design of Ti6Al4V-HA composites produced by hot pressing for biomedical applications, Mater. Des. 108 (2016) 488–493, https://doi.org/10.1016/j.matdes.2016.07.023.

[22] G.M. Peñarrieta-Juanito, M. Costa, M. Cruz, G. Miranda, B. Henriques, J. Marques, R. Magini, A. Mata, J. Caramês, F. Silva, J.C.M. Souza, Bioactivity of novel functionally structured titanium-ceramic composites in contact with human osteoblasts, J. Biomed. Mater. Res. - Part A. 106 (2018) 1923–1931, https://doi.org/10.1002/jbm.a.36394.

[23] Y. Zhang, X. Liu, Z. Li, S. Zhu, X. Yuan, Z. Cui, X. Yang, P.K. Chu, S. Wu, Nano Ag/ZnO-incorporated hydroxyapatite composite coatings: highly effective infection prevention and excellent osteointegration, Appl. Mater. Interfaces 10 (2018) 1266–1277, https://doi.org/10.1021/acsami.7b17351.

[24] J. Shen, Y. Qi, B. Jin, X. Wang, Y. Hu, Q. Jiang, Control of hydroxyapatite coating by self-assembled monolayers on titanium and improvement of osteoblast adhesion, J. Biomed. Mater. Res. - Part B Appl. Biomater. 105 (2017) 124–135, https://doi.org/10.1002/jbm.b.33539.

[25] G. Li, L. Wang, W. Pan, F. Yang, W. Jiang, X. Wu, X. Kong, K. Dai, Y. Hao, In vitro and in vivo study of additive manufactured porous Ti6Al4V scaffolds for repairing bone defects, Sci. Rep. 6 (2016) 34072, , https://doi.org/10.1038/srep34072.

[26] A. Kumar, S. Mandal, S. Barui, R. Vasireddi, U. Gbureck, M. Gelinsky, B. Basu, Low temperature additive manufacturing of three dimensional scaffolds for bone-tissue engineering applications: processing related challenges and property assessment, Mater. Sci. Eng. R. Rep. 103 (2016) 1–39, https://doi.org/10.1016/j.mser.2016.01.001.

[27] Q. Liu, Y. Wang, H. Zheng, K. Tang, L. Ding, H. Li, S. Gong, Microstructure and mechanical properties of LMD-SLM hybrid forming Ti6Al4V alloy, Mater. Sci. Eng. A 660 (2016) 24–33, https://doi.org/10.1016/j.msea.2016.02.069.

[28] B. Van Hooreweder, Y. Apers, K. Lietaert, J.P. Kruth, Improving the fatigue performance of porous metallic biomaterials produced by selective laser melting, Acta Biomater. 47 (2017) 193–202, https://doi.org/10.1016/j.actbio.2016.10.005.

[29] D. Greitemeier, F. Palm, F. Syassen, T. Melz, Fatigue performance of additive manufactured TiAl6V4 using electron and laser beam melting, Int. J. Fatigue 94 (2017) 211–217, https://doi.org/10.1016/j.ijfatigue.2016.05.001.

[30] M. Elahinia, N. Shayesteh Moghaddam, M. Taheri Andani, A. Amerinatanzi, B.A. Bimber, R.F. Hamilton, Fabrication of NiTi through additive manufacturing: a review, Prog. Mater. Sci. 83 (2016) 630–663, https://doi.org/10.1016/j.pmatsci.2016.08.001.

[31] S. Bose, D. Ke, H. Sahasrabudhe, A. Bandyopadhyay, Additive manufacturing of biomaterials, Prog. Mater. Sci. 93 (2018) 45–111, https://doi.org/10.1016/j.pmatsci.2017.08.003.

[32] R.A. Perez, G. Mestres, Role of pore size and morphology in musculo-skeletal tissue regeneration, Mater. Sci. Eng. C 61 (2016) 922–939, https://doi.org/10.1016/j.msec.2015.12.087.

[33] Straumann, Straumann SLA, Sci. Evid, First ed., 2011 (2011), pp. 1–36.

[34] P. Ming, S. Shao, J. Qiu, J. Yang, Y. Yu, J. Chen, W. Zhu, C. Tang, Superiority of calcium-containing nanowires modified titanium surface compared with SLA titanium surface in biological behavior of osteoblasts: a pilot study, Appl. Surf. Sci. 416 (2017) 790–797, https://doi.org/10.1016/j.apsusc.2017.04.152.

[35] M. Javaid, A. Haleem, Additive manufacturing applications in medical cases: a literature based review, Alex. J. Med. (2017), https://doi.org/10.1016/j.ajme.2017.09.003.

[36] F. Bartolomeu, S. Faria, O. Carvalho, E. Pinto, N. Alves, F.S. Silva, G. Miranda, Predictive models for physical and mechanical properties of Ti6Al4V produced by

selective laser melting, Mater. Sci. Eng. A 663 (2016) 181–192, https://doi.org/10.1016/j.msea.2016.03.113.

[37] R.W.N. Nilen, P.W. Richter, The thermal stability of hydroxyapatite in biphasic calcium phosphate ceramics, J. Mater. Sci. Mater. Med. 19 (2008) 1693–1702, https://doi.org/10.1007/s10856-007-3252-x.

[38] C. Wang, R. Quan, H. Wang, X. Wei, Z. Zhao, Investigation on high-temperature decomposition characteristic of hydroxyapatite, 2009 IEEE 3rd Int. Conf. Nano/Molecular Med. Eng. NANOMED, 2009 2009, pp. 65–70, , https://doi.org/10.1109/NANOMED.2009.5559116.

[39] G. Muralithran, S. Ramesh, The effects of sintering temperature on the properties of hydroxyapatite, Ceram. Int. 26 (2000) 221–230 (doi:S0272-8842(99)00046-2).

[40] ISO 4287:1997, Geometrical product specifications (GPS) – surface texture: profile method – terms, definitions and surface texture parameters, Int. Organ. Stand, https://www.iso.org/standard/10132.html, (1997).

[41] N.A. Silva, A.J. Salgado, R.A. Sousa, J.T. Oliveira, A.J. Pedro, H. Leite-Almeida, R. Cerqueira, A. Almeida, F. Mastronardi, J.F. Mano, N.M. Neves, N. Sousa, R.L. Reis, Development and characterization of a novel hybrid tissue engineering–based scaffold for spinal cord injury repair, Tissue Eng. Part A 16 (2010) 45–54, https://doi.org/10.1089/ten.tea.2008.0559.

[42] S. Ribeiro-Samy, N.A. Silva, V.M. Correlo, J.S. Fraga, L. Pinto, A. Teixeira-Castro, H. Leite-Almeida, A. Almeida, J.M. Gimble, N. Sousa, A.J. Salgado, R.L. Reis, Development and characterization of a PHBHV- based 3D scaffold for a tissue engineering and cell-therapy combinatorial approach for spinal cord injury regeneration, Macromol. Biosci. 13 (2013) 1576–1592, https://doi.org/10.1002/mabi.201300178.

[43] A. Canha-Gouveia, A. Rita Costa-Pinto, A.M. Martins, N.A. Silva, S. Faria, R.A. Sousa, A.J. Salgado, N. Sousa, R.L. Reis, N.M. Neves, Hierarchical scaffolds enhance osteogenic differentiation of human Wharton's jelly derived stem cells, Biofabrication 7 (2015) 35009, , https://doi.org/10.1088/1758-5090/7/3/035009.

[44] R. Silva, H. Ferreira, A.C. Carvalho, A.C. Gomes, A. Cavaco-Paulo, Protein microspheres as suitable devices for piroxicam release, Colloids Surf. B Biointerfaces 92 (2012) 277–285, https://doi.org/10.1016/j.colsurfb.2011.11.050.

[45] F. Bartolomeu, M. Buciumeanu, E. Pinto, N. Alves, F.S. Silva, O. Carvalho, G. Miranda, Wear behavior of Ti6Al4V biomedical alloys processed by selective laser melting, hot pressing and conventional casting, Trans. Nonferrous Metals Soc. China (2017) 829–838, https://doi.org/10.1016/S1003-6326(17)60060-8 (English ed. 27).

[46] M. Buciumeanu, A. Bagheri, N. Shamsaei, S.M. Thompson, F.S. Silva, B. Henriques, Tribocorrosion behavior of additive manufactured Ti-6Al-4V biomedical alloy, Tribol. Int. 119 (2018) 381–388, https://doi.org/10.1016/j.triboint.2017.11.032.

[47] S. Zhang, Q. Wei, L. Cheng, S. Li, Y. Shi, Effects of scan line spacing on pore characteristics and mechanical properties of porous Ti6Al4V implants fabricated by selective laser melting, Mater. Des. 63 (2014) 185–193, https://doi.org/10.1016/j.matdes.2014.05.021.

[48] A. Bandyopadhyay, F. Espana, V.K. Balla, S. Bose, Y. Ohgami, N.M. Davies, Influence of porosity on mechanical properties and in vivo response of Ti6Al4V implants, Acta Biomater. 6 (2010) 1640–1648, https://doi.org/10.1016/j.actbio.2009.11.011.

[49] B. Vrancken, L. Thijs, J.-P. Kruth, J. Van Humbeeck, Heat treatment of Ti6Al4V produced by selective laser melting: microstructure and mechanical properties, J. Alloys Compd. 541 (2012) 177–185, https://doi.org/10.1016/j.jallcom.2012.07.022.

[50] L. Ponsonnet, K. Reybier, N. Jaffrezic, V. Comte, C. Lagneau, M. Lissac, C. Martelet, Relationship between surface properties (roughness, wettability) of titanium and titanium alloys and cell behaviour, Mater. Sci. Eng. C 23 (2003) 551–560, https://doi.org/10.1016/S0928-4931(03)00033-X.

[51] N.J. Hallab, K.J. Bundy, K. O'Connor, R.L. Moses, J.J. Jacobs, Evaluation of metallic and polymeric biomaterial surface energy and surface roughness characteristics for directed cell adhesion, Tissue Eng. 7 (2001) 55–71, https://doi.org/10.1089/107632700300003297.

[52] L. Ponsonnet, V. Comte, A. Othmane, C. Lagneau, M. Charbonnier, M. Lissac, N. Jaffrezic, Effect of surface topography and chemistry on adhesion, orientation and growth of fibroblasts on nickel-titanium substrates, Mater. Sci. Eng. C 21 (2002) 157–165, https://doi.org/10.1016/S0928-4931(02)00097-8.

[53] C.-J. Chen, S.-J. Ding, C.-C. Chen, Effects of surface conditions of titanium dental implants on bacterial adhesion, Photomed. Laser Surg. 34 (2016), https://doi.org/10.1089/pho.2016.4103.

[54] M. Taborelli, M. Jobin, P. François, P. Vaudaux, M. Tonetti, S. Szmukler-Moncler, J. Simpson, P. Descouts, Influence of surface treatments developed for oral implants on the physical and biological properties of titanium. Surface characterization, Clin. Implant. Dent. Relat. Res. 8 (1997) 208–216.

[55] J. Vaithilingam, S. Kilsby, R.D. Goodridge, S.D.R. Christie, S. Edmondson, R.J.M. Hague, Functionalisation of Ti6Al4V components fabricated using selective laser melting with a bioactive compound, Mater. Sci. Eng. C 46 (2015) 52–61, https://doi.org/10.1016/j.msec.2014.10.015.

[56] G. Zhao, Z. Schwartz, M. Wieland, F. Rupp, J. Geis-Gerstorfer, D.L. Cochran, B.D. Boyan, High surface energy enhances cell response to titanium substrate microstructure, J. Biomed. Mater. Res. - Part A. 74 (2005) 49–58, https://doi.org/10.1002/jbm.a.30320.

[57] L. Le Guéhennec, A. Soueidan, P. Layrolle, Y. Amouriq, Surface treatments of titanium dental implants for rapid osseointegration, Dent. Mater. 23 (2007) 844–854, https://doi.org/10.1016/J.DENTAL.2006.06.025.

[58] E.A. Vogler, Structure and reactivity of water at biomaterial surfaces, Adv. Colloid Interf. Sci. 74 (1998) 69–117, https://doi.org/10.1016/S0001-8686(97)00040-7.

[59] R.A. Gittens, T. McLachlan, Y. Cai, S. Berner, R. Tannenbaum, Z. Schwartz, K.H. Sandhage, B.D. Boyan, The effects of combined micron-/submicron-scale surface roughness and nanoscale features on cell proliferation and differentiation, Biomaterials 32 (2011) 3395–3403, https://doi.org/10.1016/j.biomaterials.2011.01.029.The.

[60] R.N. Wenzel, Resistance of solid surfaces to wetting by water, Ind. Eng. Chem. 28 (1936) 988–994, https://doi.org/10.1021/ie50320a024.

[61] A.B.D. Cassie, S. Baxter, Wettability of porous surfaces, Trans. Faraday Soc. 40 (1944) 546–551, https://doi.org/10.1039/TF9444000546.

[62] S.P. Rodrigues, C.F.A. Alves, A. Cavaleiro, S. Carvalho, Water and oil wettability of anodized 6016 aluminum alloy surface, Appl. Surf. Sci. 422 (2017) 430–442, https://doi.org/10.1016/j.apsusc.2017.05.204.

[63] T. Motohiro, K. Yukari, S. Takahiro, Y. Yoshiyuki, N. Kaori, N. Fukue, Wettability of calcium phosphate ceramics by water, J. Ceram. Soc. Jpn. 103 (1995) 46–49.

[64] J. Lu, M. Descamps, J. Dejou, G. Koubi, P. Hardouin, J. Lemaitre, J.P. Proust, The biodegradation mechanism of calcium phosphate biomaterials in bone, J. Biomed. Mater. Res. 63 (2002) 408–412, https://doi.org/10.1002/jbm.10259.

[65] K.A. Shariff, K. Tsuru, K. Ishikawa, Fabrication of dicalcium phosphate dihydrate-coated β-TCP granules and evaluation of their osteoconductivity using experimental rats, Mater. Sci. Eng. C 75 (2017) 1411–1419, https://doi.org/10.1016/j.msec.2017.03.004.

[66] F.L. Yen, W.J. Shih, M.H. Hon, H.T. Chen, I.M. Hung, H.H. Ko, M.C. Wang, Understanding the biocompatibility of sintered calcium phosphate with ratio of [Ca]/[P] = 1.50, J. Nanomater. 2012 (2012), https://doi.org/10.1155/2012/325605.

[67] L.-E. Monfoulet, P. Becquart, D. Marchat, K. Vandamme, M. Bourguignon, E. Pacard, V. Viateau, H. Petite, D. Logeart-Avramoglou, The pH in the microenvironment of human mesenchymal stem cells is a critical factor for optimal osteogenesis in tissue-engineered constructs, Tissue Eng. Part A 20 (2014) 1827–1840, https://doi.org/10.1089/ten.tea.2013.0500.

[68] I.A. Silver, J. Deas, M. Erecińska, Interactions of bioactive glasses with osteoblasts in vitro: effects of 45S5 Bioglass(®), and 58S and 77S bioactive glasses on metabolism, intracellular ion concentrations and cell viability, Biomaterials 22 (2001) 175–185, https://doi.org/10.1016/S0142-9612(00)00173-3.